Modeling and Detection of Hotspot in Shaded Photovoltaic Cells

Daniele Rossi, Martin Omaña, Daniele Giaffreda, and Cecilia Metra, *Fellow, IEEE*

***Abstract*— In this paper, we address the problem of modeling the thermal behavior of photovoltaic (PV) cells undergoing a hotspot condition. In case of shading, PV cells may experience a dramatic temperature increase, with consequent reduction of the provided power. Our model has been validated against experimental data, and has highlighted a counterintuitive PV cell behavior, that should be considered to improve the energy efficiency of PV arrays. Then, we propose a hotspot detection scheme, enabling to identify the PV module that is under hotspot condition. Such a scheme can be used to avoid the permanent damage of the cells under hotspot, thus their drawback on the power efficiency of the entire PV system.**

***Index Terms*— Energy efficiency, hotspot, photovoltaic (PV) systems, reliability.**

I. Introduction

IN RECENT years, photovoltaic (PV) arrays have been increasingly adopted in the urban environment, as a promising source of green energy. In such an environment, (partial) shading of the PV array from nearby obstructions, such as trees, telephone poles, antennas, neighboring buildings, or from bird droppings, tree leaves, and so on, is very frequent. The shading of a PV cell or of a group of cells can lead to a phenomenon denoted as hotspot. This can produce a permanent damage of the shaded cell, with a consequent reduction of the provided power [1], [2].

Hotspot takes place when one or more PV cells within a PV module are shaded, with a consequent mismatch in the irradiation of the cells in the module. Under this condition, the nonshaded part of the module operates at current levels higher than those of the shaded PV cells. As a consequence, the affected cells are forced into reverse bias and starts to dissipate power, with a consequent temperature increase. This causes the overheating (hotspot) of the PV cells. If the shading condition is not removed before that the cell temperature reaches a critical value, the shaded PV cells can be permanently damaged [3]. In some cases, the reverse bias voltage can reach the breakdown voltage of the cell, thus leading to its destruction in a few tens of seconds [3]. As a result, an open circuit appears at the serial branch to which the cell is connected [4]. If the PV module containing the damaged cell(s) is connected in series to other PV modules, the open circuit due to the hotspot will eventually disconnect the whole branch containing the affected PV module from the PV system [4]. This will cause a considerable decrease in the energy provided by the whole PV system.

To counteract the detrimental effect of shading, bypass diodes are usually connected in antiparallel with the PV cells [2], [5] in an array. These bypass diodes limit the reverse voltage that can be applied to a PV cell, thus preventing it from reaching the breakdown voltage when shaded. However, it has been proven that hotspot conditions may still occur, even if bypass diodes are adopted [3]. Due to defects and impurities within the silicon, some PV cells may exhibit a large reverse current, even before reaching the breakdown voltage. This phenomenon is usually modeled by inserting a parallel shunt resistance, whose value depends on the concentration and distribution of defects/impurities within the PV cell. If the shunt resistance is low enough, a hotspot condition can occur even before that the PV cell enters the breakdown region [2], [3], [6]. In this case, due to the hotspot heating, the PV cell can reach a temperature high enough to cause its permanent damage [2], [3], [6], although this takes longer to occur than when the PV cell operates in breakdown.

The time required by the heating to generate a permanent damage in a PV cell under hotspot depends strongly on environmental parameters and impurities in the materials [7]. Such a time should be known to activate possible countermeasures to avoid the PV cell permanent damage, thus the consequent loss of efficiency of the whole PV array.

So far, a few approaches have been proposed to detect the hotspot condition [8], [9]. In [8] and [9], a novel PV module structure and a hotspot detection scheme are proposed. Detection is based on current monitoring, followed by a comparison with a computed theoretical value, enabling to identify the cells under hotspot. The correct computation of the current theoretical value is, however, a critical issue, given its strong dependence on environmental parameters.

Based on these considerations, in this paper we propose a new approach to detect the occurrence of hotspot to allow the application of possible countermeasures to avoid the permanent damage of the cells under hotspot. To achieve this goal, first we describe a model that we have preliminary introduced in [10], to estimate the temperature of a PV cell, as a function of the time interval in which it is under hotspot. Our model has been validated against experimental results. It shows that the time required to reach a critical temperature in the cell area under hotspot is strongly influenced by shadowing grade,

Manuscript received March 21, 2014; accepted June 9, 2014.

The authors are with the Department of Electrical, Electronic and Information Engineering, University of Bologna, Bologna 40136, Italy (e-mail: d.rossi@unibo.it; martin.omana@unibo.it; daniele.giaffreda2@unibo.it; cecilia.metra@unibo.it).

Color versions of one or more of the figures in this paper are available online at http://ieeexplore.ieee.org.

Digital Object Identifier 10.1109/TVLSI.2014.2333064

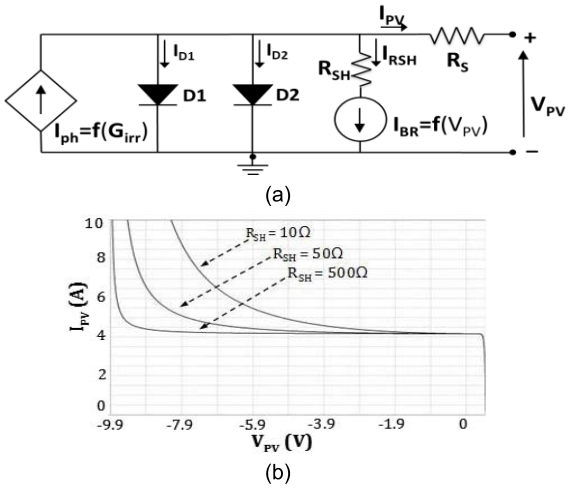

Fig. 1. (a) Considered electrical model for PV cells. (b) $I_{\rm pv}$ as a function of $V_{\rm pv}$ for three different values of $R_{\rm sh}$, with $G_{\rm irr} = 500$ W/m^2 and $I_{\rm ph} = 4$ A.

irradiation intensity, ambient temperature, and concentration of impurities in the materials.

Then, we propose a novel scheme to detect the hotspot condition affecting a cell (or multiple cells). The proposed scheme is conceived as connected to the maximum power point tracker (MPPT) of each PV module, for PV systems adopting distributed MPPT to allow the maximization of the PV system efficiency [11]. Our detection scheme enables also the quick and unambiguous identification of the PV module containing the cell(s) undergoing a hotspot condition. The output signals generated by our detection scheme can be used to activate proper countermeasures. As an example, the affected module could be properly bypassed, thus avoiding the permanent damage of the cells under hotspot and its consequent impact on the efficiency of the whole PV array. The development of such countermeasures is, however, out of the target of this paper.

The rest of the paper is organized as follows. In Section II, we introduce some basics on PV cells and hotspot heating. In Section III, we present our model to estimate the temperature of a PV cell as a function of the time interval during which it is under a hotspot condition and we validate it against experimental data. In Section IV, by applying our model, we show the thermal behavior of shaded PV cells undergoing hotspot conditions and we compare partial shading to full shading effects. In Section V, we describe our proposed hotspot detection scheme and report show some results of the simulations that we have performed to verify its behavior. Finally, in Section VI, we give some conclusive remarks.

II. PV Cell Hot-Spot Heating

A. PV Cell Electrical Model

We consider the PV cell standard double diode electrical model in [2] and [12], as shown in Fig. 1(a). When the PV cell is exposed to sunlight, it generates a photocurrent given by [13]–[15]

$$I_{\rm ph} = (J_{\rm ph} \cdot A_{\rm cell} \cdot G_{\rm irr})/G_{\rm max} \tag{1}$$

where $G_{\rm irr}$ [W/m^2] is the solar irradiation, $J_{\rm ph} = 3.43$ [μA/m^2] is the maximum photocurrent density for the maximum solar radiation $G_{\rm max} = 1000$ W/m^2 and $A_{\rm cell}$ [m^2] is the area of the PV cell. Diodes $D1$ and $D2$ account for the saturation mechanisms in the PV cell [1], [8]. In particular, I_{D1} is the saturation current due to the diffusion mechanism, while I_{D2} is the saturation current generated by the recombination in the space charge layer. The current $I_{\rm RSH}$ represents the leakage current of the PV cell, which is accounted for by the shunt resistance $R_{\rm SH}$ [2], [13]. The resistance R_S models the voltage drop across the PV cell produced by the current $I_{\rm PV}$ [8]. Therefore, the current $I_{\rm PV}$ provided by the PV cell to its load is given by

$$I_{\rm PV} = I_{\rm ph} - I_{D1} - I_{D2} - I_{\rm RSH}. \tag{2}$$

When a PV cell is biased in the reverse breakdown region, its behavior is modeled by the current generator $I_{\rm BD}$, whose produced current is controlled by the output voltage $V_{\rm PV}$. In detail, $I_{\rm BD}$ is approximately equal to 0 A for values of $V_{\rm PV}$ higher than the cell breakdown voltage ($V_{\rm BD}$). Instead, for values of $V_{\rm PV}$ lower than $V_{\rm BD}$ [2], it is

$$I_{\rm BD} \cong \alpha \cdot (V_{\rm PV}/R_{\rm SH}) \cdot (1 - (V_{\rm PV}/V_{\rm BD}))^{-m}.$$

Parameters α and m are fitting parameters having the following values: $\alpha = 1.93$ and $m = 1.10$ [2].

Fig. 1(b) shows the current $I_{\rm PV}$ as a function of $V_{\rm PV}$, for a PV cell modeled by the circuit in Fig. 1(a). The curves have been derived considering a solar irradiation $G_{\rm irr} = 500$ W/m^2, generating a photocurrent $I_{\rm ph} = 4$ A, and three different values of the shunt resistance $R_{\rm SH}$. When $V_{\rm PV} = 0$ V, it is $I_{\rm PV} = I_{\rm ph} = 4$ A. In this case, no current flows through $R_{\rm SH}$ ($I_{\rm RSH} = 0$) and $D1$ and $D2$ are OFF ($I_{D1} = I_{D2} = 0$). In addition, also when $0 < V_{\rm PV} < 0.6$ V, it is $I_{\rm PV} \approx I_{\rm ph}$, since $D1$ and $D2$ are still OFF and $I_{\rm RSH}$ is very small. Instead, for $V_{\rm PV} > 0.6$ V, the current $I_{\rm PV}$ start to decrease quickly as $V_{\rm PV}$ increases, since $D1$ and $D2$ become conductive, and I_{D1} and I_{D2} increase quickly as $V_{\rm PV}$ increases. From Fig. 1(b), we can also observe that, when the PV cell is reverse biased ($V_{\rm PV} < 0$), the current $I_{\rm PV}$ increases with the decrease of $V_{\rm PV}$. In addition, it can be noticed that the value of $I_{\rm PV}$ strongly depends on the value of the shunt resistance $R_{\rm SH}$. In particular, $I_{\rm PV}$ increases faster, when the value of $R_{\rm SH}$ diminishes.

It is worth noticing that, when the PV cell is reverse biased, the absolute value of $V_{\rm PV}$ can be as high as 10 V, so that the power dissipated by the PV cell can be very high [2] and the temperature of the PV cell can considerably increase.

When the PV cell is reverse biased, $I_{\rm PV}$ is nonhomogeneously distributed throughout the cell area and concentrates in small regions (with an area approximately equal to 100 μm^2) of slightly higher conductivity, where the silicon presents a higher concentration of defects/impurities [3], [7], [16].

This physical phenomenon is considered in the value of the shunt resistance $R_{\rm SH}$. A low value of $R_{\rm SH}$ will originate a large value of $I_{\rm PV}$ when the cell is reverse biased, which will produce a high-power dissipation on $R_{\rm SH}$. Such a power dissipation can produce a considerable increase in the temperature of the regions of the PV cell that are close to the impurity centers, thus giving rise to hotspot heating

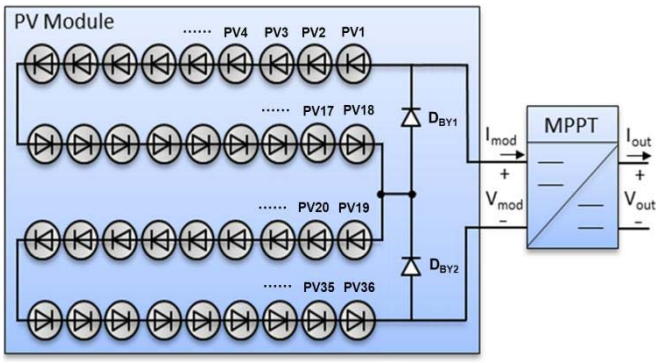

Fig. 2. Considered PV module architecture with distributed MPPT.

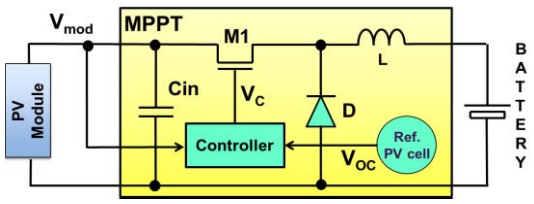

Fig. 3. Schematic view representation of the considered step-down buck converter implementing the MPPT circuit.

[6], [12]. Under hotspot, the temperature of the heated regions can exceed the maximum value tolerated by the PV cell and can be permanently damaged [2], [3], [6].

To enter a hotspot condition, a PV cell must be reverse biased. This is likely to occur in typical PV arrays, where many PV cells are connected in series to obtain an adequate level of dc voltage [9], [17].

B. PV Module Architecture and MPPT Scheme

Several PV module and array architectures have been proposed in [11], [18], and [19]. We here consider the approach based on distributed MPPT since, as highlighted in [11], it allows to maximize the PV system efficiency.

1) PV Module Architecture With Distributed MPPT: We consider the PV array scheme as shown in Fig. 2 [11]. It is composed by a series of 36 identical PV cells (PV_i, $i = 1, \ldots, 36$), with two bypass diodes (DBYP_i, $i = 1, 2$), each connected in parallel to 18 PV cells [2]. The bypass diodes avoid that a shaded PV cell, which is reverse biased, can enter its breakdown region. The reverse voltage of a shaded PV cell within the array in Fig. 2, which is equal to the sum of the forward voltages of the other 17 nonshaded PV cells sharing the same bypass diode, is always lower than its breakdown voltage V_{BR} (typically equal to -10 V).

2) Maximum Power Point Tracker: The MPPT absorbs the dc power from the PV array and transfers it to the battery. The main function of the MPPT is to adjust the current and voltage of the PV module, denoted by I_{mod} and V_{mod}, respectively (Fig. 2), to maximize the power produced by the PV array for any given solar irradiation G_{irr}.

The MPPT is usually implemented by means of a dc–dc converter [5], [13], [14], such as the step down dc–dc buck converter shown in Fig. 3, which allows to convey the power produced by the PV module to the battery. It is composed by a transistor $M1$ acting as a switch and a freewheeling diode D. As for the components L and C_{in}, they filter out spikes on the current provided to the battery and oscillations on the voltage V_{mod} produced by the PV module, respectively, both induced by the switching of $M1$ and D.

The controller generates a periodic control signal (V_C) with variable duty-cycle allowing to modulate the time during which $M1$ is ON, during each period of V_C. This enables to control the average current absorbed from the PV module, as well as the voltage V_{mod}, thus making the PV module work at its maximum power point (MPP). In our example, the controller implements the open-voltage tracking method [15], [17] that, for its simple implementation and low cost, is often employed in PV systems [15]. This method exploits the linear relationship existing between the voltage at which a cell maximizes the generated power (V_{MPP}) and its open circuit voltage (V_{OC}). In particular, it is always $V_{\mathrm{MPP}} = 0.76\ V_{\mathrm{OC}}$, for any solar irradiation G_{irr}. Therefore, to make the cells of the PV module work at their MPP, the controller compares the voltage of the cells of the array (V_{cell}) with the V_{OC} of a reference cell operating under the same G_{irr} as the PV module. Based on the comparison result, the controller adjusts the duty-cycle of V_C so that $V_{\mathrm{cell}} = 0.76$ and $V_{\mathrm{OC}} = V_{\mathrm{MPP}}$ [16]. Finally, to obtain V_{cell}, the controller simply divides the voltage V_{mod} by the number of cells connected in series in the module.

III. Model Description and Validation

As described in Section II, when one PV cell within a series of PV cells is shaded, the power generated by the reverse current of the cell is therefore dissipated in a small area close to impurity centers [7]. Fig. 4(a) shows a representation of the shaded PV cell. The area of the whole PV cell is denoted by A_{cell}, while the area of the regions involved by hotspot heating is denoted by A_{HS}. In particular, A_{HS} represents the area of the region of the PV cell around the impurity centers experiencing a considerable temperature increase when the PV cell is partially/fully shaded. The value of A_{HS} depends on the PV cell fabrication process and has been experimentally proven to be usually in the range of 5%–10% of A_{cell} [20].

Our model, as preliminarily described in [10], consists of two series thermal RC circuits. The lower RC circuit (composed by C_{THcell} and R_{THcell}) accounts for the temporal behavior of the PV cell temperature as a function of solar irradiation [T_{cell} in Fig. 4(b)] only. Instead, the upper thermal RC circuit (composed by $C_{\mathrm{TH-HS}}$ and $R_{\mathrm{TH-HS}}$) models the temporal behavior of the area A_{HS} of the PV cell under hotspot condition, as a function of the power dissipated (P_{diss}) on the shunt resistor R_{SH}. In particular, P_{diss} is estimated by SPICE simulations as the power dissipated on the shunt resistance, that is, $P_{\mathrm{diss}} = R_{\mathrm{SH}} \cdot I_{\mathrm{SH}}^2$ [W/m^2], where I_{SH} is the reverse bias current of the shaded PV cell.

As for the other parameters in Fig. 4(b), T_{HS} [°C], $R_{\mathrm{TH-HS}}$ [°C $\cdot$ m^2/W], and $C_{\mathrm{TH-HS}}$ [°C $\cdot$ m^2 $\cdot$ s/W] are the temperature, thermal resistance, and thermal capacitance, respectively, of the PV cell portion A_{HS}, T_{cell} [°C], R_{THcell} [°C $\cdot$ m^2/W], and

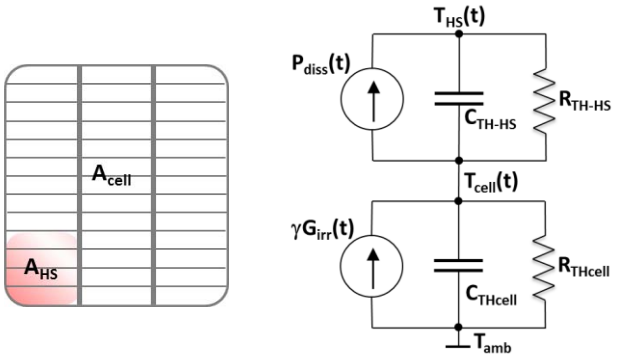

(a) (b)

Fig. 4. (a) Partial shaded PV cell undergoing hotspot condition. (b) Equivalent thermal model to estimate the time dependence of the temperature of the portion of the PV cell (A_{HS}) under hotspot condition.

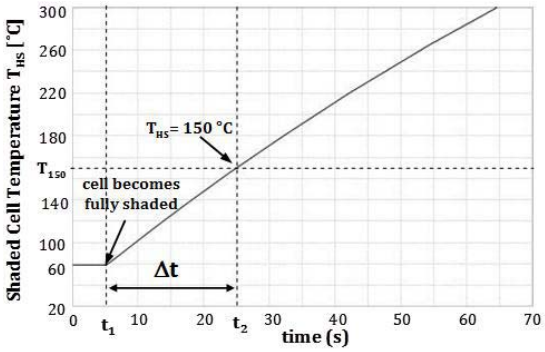

Fig. 5. Temperature trend over time in the fully shaded cell, for the operating conditions reported in [23].

C_{THcell} [°C · m^2· s/W] are the temperature, thermal resistance, and thermal capacitance, respectively, of the remaining portion (not undergoing a hotspot condition) of the shaded PV cell, T_{amb} [°C] is the ambient temperature, G_{irr} [W/m^2] is the solar radiation density illuminating the PV cell.

The values of parameters $R_{\mathrm{TH-HS}}$, R_{THcell}, $C_{\mathrm{TH-HS}}$, and C_{THcell} depend on the materials composing the upper layers of the PV cell (i.e., mainly EVA, glass, etc.). Since most of the heat produced by the PV cell is dissipated on the glass layer [21], we can reasonably assume that the values of these parameters depend only on the properties of the glass layer covering the cell. Therefore, they can be calculated as follows [21]:

$$\begin{aligned} R_{\mathrm{THcell}} &= \frac{l}{k \cdot A_{\mathrm{cell}}} \\ R_{\mathrm{TH-HS}} &= \frac{l}{k \cdot A_{\mathrm{HS}}} \\ C_{\mathrm{THcell}} &= A_{\mathrm{cell}} \cdot l \cdot \rho \cdot \varsigma \\ C_{\mathrm{TH-HS}} &= A_{\mathrm{HS}} \cdot l \cdot \rho \cdot \varsigma \end{aligned} \tag{3}$$

where l [m] is the thickness of the glass covering the PV cell, k is the glass thermal conductivity, ρ [Kg/m^3] is the glass density, and ς [J/Kg · °C] is the glass specific heat capacity.

From the thermal circuit in Fig. 4(b), we can derive the behavior over time of the temperature T_{HS} in the area of the PV cell that is shaded, thus undergoing a hot-sport condition, at a generic time instant denoted by t_{HS}, as follows:

$$T_{\mathrm{HS}}(t) = \begin{cases} T_{\mathrm{amb}} + R_{\mathrm{THcell}} G_{\mathrm{irr}} & t < t_{\mathrm{HS}} \\ T_{\mathrm{amb}} + R_{\mathrm{THcell}} G_{\mathrm{irr}} \left(\gamma + (1-\gamma) e^{-\left(\frac{t-t_{\mathrm{HS}}}{R_{\mathrm{THcell}} C_{\mathrm{THcell}}}\right)}\right) & \\ \quad + P_{\mathrm{diss}} R_{\mathrm{TH-HS}} \left(1 - e^{-\left(\frac{t-t_{\mathrm{HS}}}{R_{\mathrm{TH-HS}} C_{\mathrm{TH-HS}}}\right)}\right) & t \geq t_{\mathrm{HS}} \end{cases} \tag{4}$$

where $\gamma = G_{\mathrm{irr-shaded}}/G_{\mathrm{irr}}$ denotes the relative mismatch in the irradiation between the shaded ($G_{\mathrm{irr-shaded}}$) and nonshaded (G_{irr}) cells of the PV array. Thus, a fully shaded PV cell will present $\gamma = 0$, while for nonshaded PV cells it is $\gamma = 1$.

It is worth noting that the time t_{HS} represents the (arbitrary) generic instant when a hotspot condition occurs. For $t < t_{\mathrm{HS}}$ (that is before the PV cell is shaded and enters a hotspot condition), the cell works with the same solar irradiation G_{irr} as the other PV cells in the panel, with $\gamma = 1$, so that it is forward biased. In this case, it is $P_{\mathrm{diss}} = 0$, and $A_{\mathrm{HS}} = 0$, and the equivalent circuit coincides with the lower RC circuit in Fig. 4(b). Therefore, the cell temperature turns out to depend only on the solar irradiation. It is

$$T_{\mathrm{HS}} = T_{\mathrm{cell}} = T_{\mathrm{amb}} + R_{\mathrm{THcell}} \cdot G_{\mathrm{irr}}.$$

On the other hand, we can observe that after the PV cell is shaded and enters a hotspot condition (for $t \geq t_{\mathrm{HS}}$), there are two different phenomena determining the temperature of the PV cell: 1) the contribution of the reduced solar irradiation [i.e., the second term in (4) for $t \geq t_{\mathrm{HS}}$], which tends to reduce the PV cell temperature with a time constant $\tau_{\mathrm{cell}} = R_{\mathrm{THcell}} \cdot C_{\mathrm{THcell}} = l \cdot \rho \cdot \varsigma / k$ [s]; and 2) the contribution of the power dissipated by R_{SH} (P_{diss}) [i.e., the third term in (4) for $t \geq t_{\mathrm{HS}}$], which tends to increase the PV cell temperature with a time constant $\tau_{\mathrm{HS}} = R_{\mathrm{TH-HS}} \cdot C_{\mathrm{TH-HS}} = l \cdot \rho \cdot \varsigma / k$ [s]. As shown in [10], the contribution of 2) to the temperature T_{HS} is considerably higher than the contribution of 1). As a result, when a PV cell is shaded, its temperature T_{HS} tends to increase very quickly.

Our thermal model [Fig. 4(b)] can be simulated by means of electrical simulation tools, such as SPICE. To this aim, the units of the obtained voltages (currents) must be converted to temperature (power) units, so that 1 V (1 A) in the simulated electrical circuit corresponds to 1 °C (1 W) in the thermal circuit. To summarize, our model allows to evaluate simply and quickly the maximum time interval in which a PV cell can remain under a hotspot condition, without suffering from permanent damages due to excessive temperature.

We have compared the results obtained using our model to the experimental data reported in [22] and [23], considering the same operating conditions and the cell parameters in [22]. Fig. 5 shows the temperature behavior of a shaded cell obtained by our model. We can observe that, before the cell is shaded at time t_1, it presents a constant operating temperature of 60 °C, with an ambient temperature of 25 °C. This is

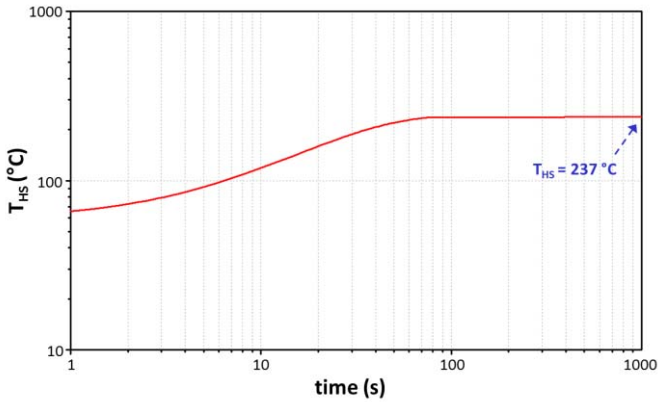

Fig. 6. Temperature trend over time in the fully shaded cell, for the operating conditions reported in [24].

in very good agreement with the operating temperature of a nonshaded PV cell reported in [22], which reaches $T = 57.2$ °C with an ambient temperature of 20 °C. After the cell is shaded (at time t_1), our model estimates a time interval $\Delta t = t_1 - t_2 = 21.1$ s for the operating temperature of the area of the cell under hotspot to rise by 90 °C, thus reaching a temperature of 150 °C. This result is also in accordance with the experimental data in [23], which reports a thermal behavior of e cell under hotspot exhibiting a temperature increase of 90 °C in approximately 18 s. The small difference is due to the different PV cell parameters. Therefore, the proposed model allows to predict the time required by a PV cell to enter a hotspot condition rather accurately.

We further validated the proposed model with the results reported in [24]. We considered the same power dissipation of 15.1 W in the hotspot area of the shaded PV cell. The obtained results are shown in Fig. 6. As can be seen, after 1000 s, a temperature variation equal to $\Delta T = (237-60)$ °C = 177 °C is achieved, while in [24] a $\Delta T = 183$ °C is reported. Therefore, the proposed model enables an accurate evaluation of the thermal transient of a PV cell undergoing a hotspot condition.

IV. Thermal Behavior Derived From Our Model

In this section, we have considered the same PV module shown in Fig. 2. As an example, for our analysis we have assumed that the cell PV36 is either almost fully shaded ($\gamma = 0.01$) or partially shaded ($\gamma = 0.3$). Of course similar results would have been obtained considering another PV cell in the module.

We have modeled the PV cells of the module with the electrical circuit shown in Fig. 1(a), considering the following values for its parameters [5]: $V_{BD} = -10$ V, $\alpha = 1.93$, $m = 1.10$, $R_{SH} = 139.6\ \Omega$, and $R_S = 10\ \text{m}\Omega$. In addition, for each one of the 18 PV cells, we have considered a typical area of $A_{cell} = 243\ \text{cm}^2$, from which we can derive a typical $A_{HS} = 14\ \text{cm}^2$, equal to the 6% of A_{cell} [20].

Then, in (3), the following parameter values are obtained: $R_{THcell} = 1.4$ °C/W, $R_{TH-HS} = 14$ °C/W, $C_{THcell} = 65.5$ Ws/°C, and $C_{TH-HS} = 6.5$ Ws/°C. At first step, by means of electrical level simulations performed by SPICE, we have estimated the power dissipation on the shunt resistance R_{SH} of the shaded PV cell (i.e., PV36) for the two considered cases: 1) when PV36 is almost fully shaded ($\gamma = 0.01$); and 2) when PV36 is partially shaded ($\gamma = 0.3$). The obtained values of dissipated power have then been employed in our thermal model [Fig. 4(b) and (6)] to evaluate the temperature T_{HS} of the shaded cell PV36, as a function of time. In particular, we have used our model to evaluate the time required by the temperature T_{HS} of PV36 to reach 150 °C (hereafter denoted by T_{150}) from the beginning of its partial/full shading, where T_{150} is the minimal value of temperature that can cause permanent damage to the PV cell, in case of hotspot heating [6].

Fig. 7(a) shows the results obtained in case of full shading ($\gamma = 0.01$) of PV36 and for different values of its shunt resistance R_{SH}. In particular, we considered five possible values of R_{SH}, with a $\pm 20\%$ variation with respect to its nominal value. As stated in Section II, the shunt resistance may considerably vary for different impurity concentrations and distributions within a PV cell [7], [16]. The initial irradiation is uniform for the whole module at the maximum value $G_{irr} = 1000\ \text{W/m}^2$ and the produced temperature is $T_{HS} = 60$ °C on all cells. At instant $t_{1FS} = 5$ s the cell PV36 is completely shaded ($G_{irr} = 10\ \text{W/m}^2$), while the other cells keep on being fully irradiated (thus obtaining $\gamma = 0.01$). As can be seen, the time interval Δt_{FS} required by T_{HS} to reach the critical temperature T_{150} (at time t_{2FS}) strongly depends on the value of R_{SH}. In the worst case (represented by the lowest value of $R_{SH} = 112\ \Omega$), it is, $\Delta t_{FS} = t_{2FS} - t_{1FS} = 40$ s. For larger values of R_{SH}, Δt_{FS} decreases, being approximately $\Delta t_{FS} = 65$ s for the highest value of $R_{SH} = 167\ \Omega$.

Similarly, Fig. 7(b) shows the trend over time of the T_{HS} of PV36 when, starting from the time instant $t_{1PS} = 5$ s, it is partially shaded (with $G_{irr} = 300\ \text{W/m}^2$, thus $\gamma = 0.3$), for $R_{SH} = 112\ \Omega$ [i.e., R_{SH} fixed at the lowest value considered in Fig. 7(a)]. It is worth noticing that the temperature of the partially shaded cell PV36 increases faster than that of the fully shaded cell shown in Fig. 7(a). In particular, it is $T_{HS} = T_{150}$ after a time interval equal to $\Delta t_{PS} = t_{2PS} - t_{1PS} = 36\ \text{s} < \Delta t_{FS}$. This counterintuitive behavior highlighted by our model can be explained from a physical point of view by considering that, in the partially shaded cell, the full irradiation of part of the cell shortens the time needed to enter the hotspot condition.

V. Proposed Hot-Spot Detection Scheme

In this section, we propose a scheme to detect a hotspot condition affecting a cell (or multiple cells) within a PV module. Our scheme is based on the observation that, when a hotspot condition occurs (due to full or partial shading), the current provided by the PV module, I_{mod}, varies considerably depending on the shading condition.

On the other hand, the voltage V_{mod} is maintained at a constant value by the MPPT. The controller block of the MPPT regulates the control signal V_C (Fig. 3) to maintain the voltage V_{mod} equal to 0.76 V_{OC}, where V_{OC} is the open circuit voltage of a reference cell.

In this regard, let us consider the case of a cell of a PV module (Fig. 2) being partially shaded. The simulation results

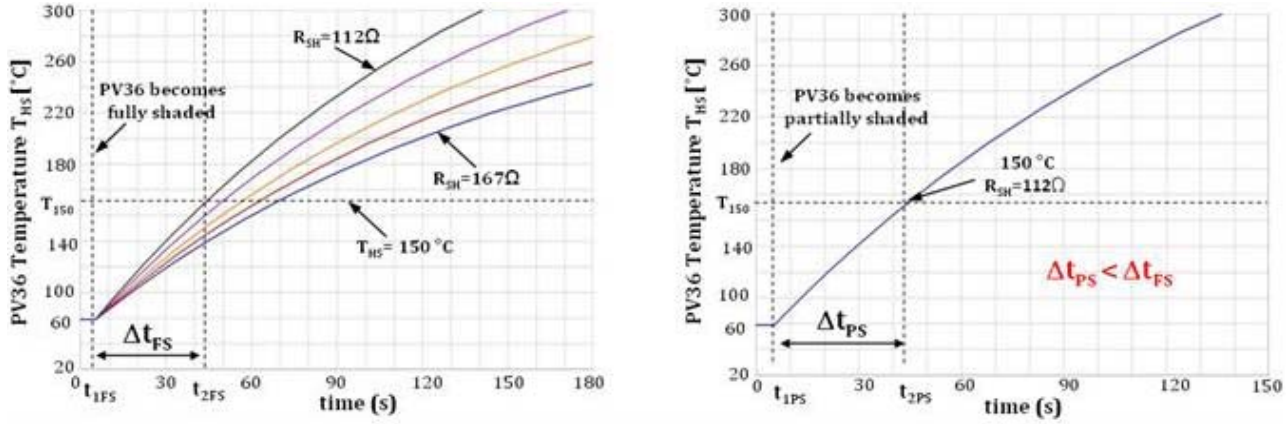

(a) (b)

Fig. 7. Results obtained with our model for the behavior of the T_{HS} temperature of PV36 when (a) PV36 becomes fully shaded after $t_{1\mathrm{FS}} = 5$ s ($\gamma = 0.01$) and for various values of R_{SH} and (b) PV36 becomes partially shaded after $t_{1\mathrm{PS}} = 5$ s (with $\gamma = 0.3$) and with the lowest value of $R_{\mathrm{SH}} = 112\ \Omega$ (worst case condition for the cell temperature).

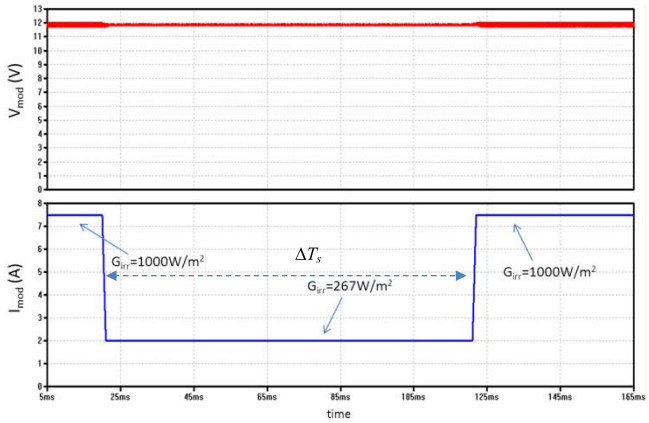

Fig. 8. Simulation results showing the behavior of the current I_{mod} and the voltage V_{mod} of the PV module in Fig. 2 when one of its PV cells becomes partially shaded.

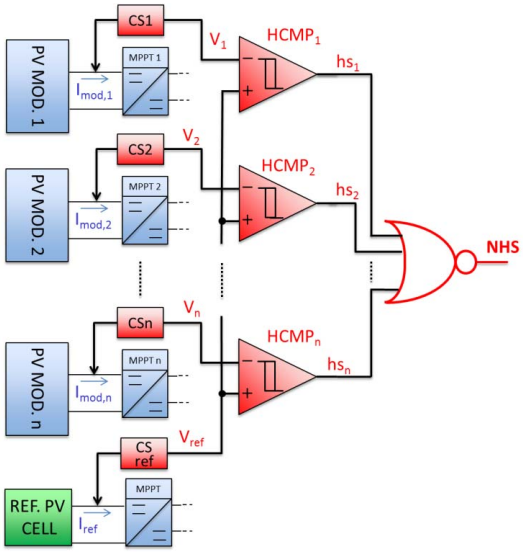

Fig. 9. Schematic view representation of the proposed hotspot detection scheme.

are shown in Fig. 8. As can be seen, when the irradiation of the shaded cell decreases from $G_{\mathrm{irr}} = 1000$ to 267 W/m^2, the current provided by the module drops from 7.5 to 2 A. This value is maintained as long as the shading condition persists, that is during the time interval ΔT_s, after which the correct current value is recovered. Instead, we can observe that V_{mod} is kept to a constant value also while the shading condition occurs. Then, as soon as the shading is removed, the previous value of I_{mod} is restored.

From the simulation results in Fig. 8, we can deduce that V_{mod} is not suitable to be monitored to detect possible hotspots, due to its negligible variation after the occurrence of a shading condition. Reversely, the current I_{mod} is affected considerably as long as the shading condition persists. Therefore, as anticipated above, our proposed detection scheme is based on the idea to monitor the I_{mod} current.

A. Hot-Spot Detection Scheme Structure

The structure of the proposed detection scheme is shown in Fig. 9. A current sensor CS_i ($i = 1, \ldots, n$) is connected to the output of each PV module PVMOD_i ($i = 1, \ldots, n$). Each current sensor CS_i gives as output a voltage V_i that is proportional to the current $I_{\mathrm{mod},i}$ sensed at the PVMOD_i output. The voltage V_i is then compared, by means of an hysteresis comparator (HCMP_i), to a reference voltage (V_{ref}) provided by a reference current sensor $\mathrm{CS}_{\mathrm{ref}}$. The sensor $\mathrm{CS}_{\mathrm{ref}}$ measures the current (I_{ref}) produced by a reference cell. The measured current is equal to the current produced by the PV modules PVMOD_i ($i = 1, \ldots, n$) under the same irradiation conditions. Of course, the reference cell should be properly selected, in order to be exempt from systematic shading, for instance due to the surrounding environment (e.g., antennas, trees, etc.), as well as from casual shading events (e.g., tree leaves, bird drops, etc.). The output of comparators HCMP_i (hs_i) are then collected by a NOR gate, which generates an alarm signal NHS if at least one module undergoes a hotspot condition.

The sensor must not alter the value of the power provided by the PV module to the respective MPPT block, in order not to affect the power efficiency of the whole PV system. Therefore, as discussed in the following section, the current

sensors CS_i have been implemented by means of Hall effect sensors [25]. They sense the magnetic field induced by the current generated by the PV module and produce an output voltage proportional to the sensed magnetic field.

In detail, the hysteresis comparators $HCMP_i$ produce at their outputs hs_i

$$\begin{aligned} hs_i &= 0(0V), \quad \text{if } I_{\text{mod},i} \geq I_{\text{ref}} \qquad (V_i = kI_{\text{mod},i} \geq V_{\text{ref}} = kI_{\text{ref}}) \\ hs_i &= 1(V_{\text{cc}}), \quad \text{if } I_{\text{mod},i} < I_{\text{ref}} - I_{\text{th}} \\ &\qquad (V_i = kI_{\text{mod},i} < V_{\text{ref}} - V_{\text{th}} = k(I_{\text{ref}} - I_{\text{th}}) \end{aligned} \tag{5}$$

where I_{th} is a proper threshold current and k [V/A] is the equivalent transresistance of the Hall effect current sensors. As shown later, the value of I_{th} must be chosen by evaluating the minimum value of the radiation density G_{irr} during a shading condition giving rise to a hotspot.

This way, if all PV modules and the reference cell are equally irradiated, then all PV modules produce a current value equal to I_{ref}, and all comparators $HCMP_i$ give to their outputs $hs_i = 0\ \forall i = 1, \ldots, n$. Therefore, the detection scheme output NHS remains at its high-logic value (NHS = 1), denoting that no hotspot condition has occurred.

Instead, if the ith PV module undergoes a hotspot condition, the provided current $I_{\text{mod},i}$ turns out to be lower than I_{ref}. As a consequence, the output of the ith comparator, hs_i, switches to 1 and the output of the detection scheme NHS goes to zero, thus generating a hotspot alarm.

It is worth noticing that the signals hs_i can also be employed for diagnosis purposes. They allow to identify the PV module undergoing a hotspot condition. Therefore, when NHS = 0 (hotspot alarm), a proper recovery mechanism can be activated (for instance based on bypassing the affected PV module), thus allowing to avoid the permanent damage of the cells under hotspot, and therefore their impact on the power efficiency of the entire PV system.

It should be noted that, since the proposed hotspot detection approach relies in the comparison between current/voltage of the PV module and a reference PV cell, its application is not limited by the considered MPPT method. In particular, if the frequently used approach based on perturb and observe [26] is considered, we can reasonably expect that the difference between the values of current/voltage of the monitored PV module and the reference one is always smaller than the mismatch tolerated by the proposed hotspot detection scheme (Fig. 9).

B. Proposed Scheme Implementation and Validation

We have implemented and validated the proposed hotspot detection scheme by means of SPICE simulations. The implemented PV modules to be monitored consist of 36 series cells (Fig. 2), modeled as described in Section II. The same model has been used to implement the reference PV cell. We have implemented the MPPT connected to each monitored PV module and to the reference cell as described in Section II-B (Fig. 3).

The hysteresis behavior of the $HCMP_i$ block described in (5) has been obtained as represented in Fig. 10. The voltage V_{ref} generated by the reference circuit is diminished by a threshold $V_{\text{th}} = kI_{\text{th}}$ by means of a standard subtractor SUB. Then, the obtained value $V'_{\text{ref}} = V_{\text{ref}} - V_{\text{th}}$ is given to the input of a standard comparator CMP_i of the kind in [27], together with the value V_i coming from the current sensor of the $PVMOD_i$ ($i = 1, \ldots, n$) module.

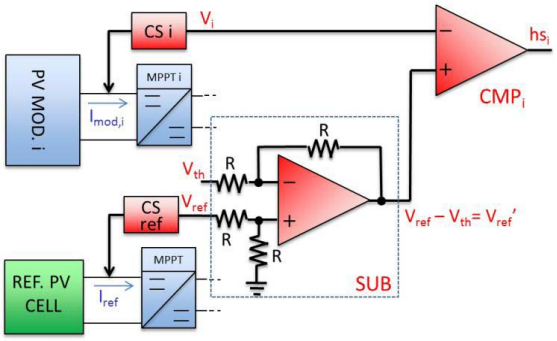

Fig. 10. Proposed implementation of the hysteresis comparators in $HCMP_i$.

As for the current sensors CS_i ($i = 1, \ldots, n$) and CS_{ref} in Fig. 9 they have been implemented by means of Hall effect current sensors of the kind in [25]. Each sensor measures indirectly the current produced by the PV array by measuring its associated magnetic field [25]. Then, as indicated in (5), the sensors give to their outputs a voltage $V_i = kI_{\text{mod},i}$ ($i = 1, \ldots, n$), where k is the equivalent transresistance of the Hall effect current sensors. As power supply, we have used a voltage of 5 V. All signals produced by the comparators (hs_i, $i = 1, \ldots, n$) feed a NOR gate generating an indication of hotspot affecting a PV cell. This way, it is NHS = 1 (i.e., 5 V), if none of the cells of a PV module is affected by a hotspot condition, or NHS = 0 (i.e., 0 V), when one (or more) PV cells of a module is (are) under hotspot.

We have performed electrical simulations to determine the threshold $V_{\text{th}} = kI_{\text{th}}$, where $k = 667$ mΩ, for which the irradiation density G_{irr} of a shaded cell undergoing a hotspot condition gives rise to a temperature increase up to 150 °C. This irradiation value has been denoted by $G_{\text{irr}-150}$.

In particular, within a PV module, the cell with a low-shunt resistance undergoing a hotspot condition is uniformly shaded, while the rest of the cells in the PV module are fully irradiated with $G_{\text{irr}} = 1000$ W/m^2. The obtained results are shown in Fig. 11. For $G_{\text{irr}} = 1000$ W/m^2, the operating temperature is 60 °C. As the G_{irr} of the low-shunt resistance shaded cell (undergoing a hotspot condition) decreases, the generated current decreases as well. As a consequence, the reverse voltage applied to the shaded cell turns out to increase (in absolute value). Therefore, also the power dissipated in the low-shunt resistance area increases, rising up the temperature of the cell area undergoing a hotspot condition. In particular, the irradiation density $G_{\text{irr}-150}$ is equal to 972 W/m^2. Afterward, the threshold current I_{th} has been obtained by introducing $G_{\text{irr}-150}$ in (1), and by simulating the circuit in Fig. 1(a). As a result, a value of $V_{\text{th}} = 200$ mV has been derived.

Fig. 12 shows some results of the simulation performed to validate the proposed hotspot dentection scheme. For simplicity, only the value of the reference cell and

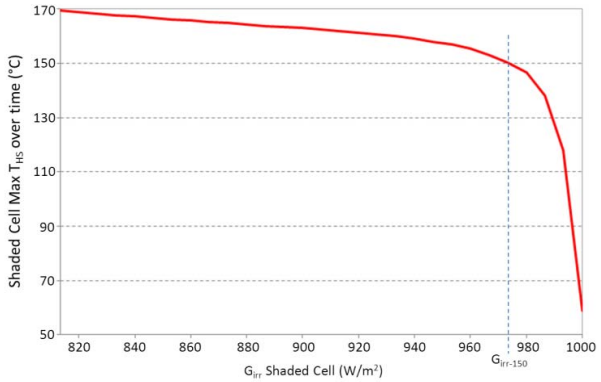

Fig. 11. Temperature increase in the cell area under hotspot in a shaded cell as a function of the cell irradiation density.

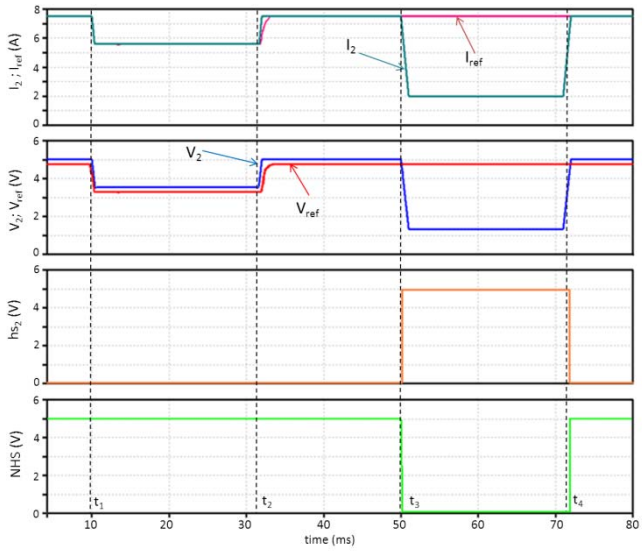

Fig. 12. Simulation results showing the behavior of the proposed hotspot detection scheme in case of uniform shading (t_1–t_2), normal irradiation (t_2–t_3), and hot spot-condition (t_3–t_4).

the PV module PV-MOD$_2$ are shown. As an example, at the instant t_1, we have emulated the occurrence of a uniform shading of the whole PV system with a $G_{\text{irr}} = 746$ W/m^2, which can for instance occur in a cloudy day. As can be seen, the output currents of both the reference cell and the monitored PV modules decrease from 7.5 A (the value corresponding to $G_{\text{irr}} = 1000$ W/m^2) to 5.6 A. Meanwhile, the output voltages provided by the current sensors connected to PV-MOD$_2$ (V_2) and $V'_{\text{ref}} = V_{\text{ref}} - V_{\text{th}}$ decrease, yet maintaining the voltage difference V_{th} they presented before t_1. In this case, the comparator HCMP$_2$ keeps on producing $\text{hs}_2 = 0$, and the alarm signal NHS remains high, indicating a hotspot free condition. The same considerations hold true between t_2 and t_3, where the maximum G_{irr} is again reached.

Instead, after the instant t_3, a hotspot condition affecting PV-MOD$_2$ occurs and the current generated by PV-MOD$_2$ drops to a value considerably lower than that produced by the reference cell. Similarly, the output signal of the current sensor CS2 diminishes to a value lower than V'_{ref}. As a consequence, the output produced by the comparator HCMP$_2$ switches from 0 to 1, and the output NOR gate generates the alarm signal $\text{NHS} = 0$. The correct behavior of PV-MOD$_2$ is recovered as soon as the shading conditions inducing a hotspot are removed after the time instant t_4.

The detection of a hotspot condition is the first step toward the possible activation of countermeasures to counteract this phenomenon. In this regard, to avoid permanent efficiency loss, after the detection of a hotspot condition, the affected PV module could be by-passed by activating a proper switch [18], [19]. Then, after some time, a verification procedure could be activated to verify whether the hotspot conditions still persist. If this is the case, a procedure for the manual removal of the hotspot condition could be actuated. The bypass of the PV module experiencing a hotspot will introduce a temporary efficiency loss, but it will prevent the PV module from incurring a permanent damage, thus avoiding a permanent efficiency loss.

VI. Conclusion

We first have addressed the problem of modeling the thermal behavior of PV cells that, due to their being exposed to shading, may experience a dramatic temperature increase (a phenomenon referred to as hotspot) with consequent reduction of the provided power. Our model has been validated against experimental data. It has highlighted that, differently from what may be expected, a partially shaded PV cell enters the hotspot condition faster than a fully shaded PV cell, thus providing useful hints that should be considered to design a highly energy efficient PV array.

We have then proposed a hotspot detection scheme, which has been validated by means of electrical level simulations. Our scheme allows to detect the occurrence of a hotspot affecting one of the PV module of the considered PV system and to identify the affected module. This enables the possible activation of proper recovery mechanisms aimed at avoiding the damage of the module under hotspot, as well as the drawback of the PV module under hotspot on the power efficiency of the entire PV power generator system.

References

[1] A. Kovach and J. Schmid, "Determination of energy output losses due to shading of building-integrated photovoltaic arrays using a raytracing technique," *Solar Energy*, vol. 57, no. 2, pp. 117–124, 1996.

[2] M. C. A. García, W. Herrmann, W. Bohmer, and B. Proisy, "Thermal and electrical effects caused by outdoor hot-spot testing in associations of photovoltaic cells," *Progr. Photovolt., Res. Appl.*, vol. 11, no. 5, pp. 293–307, 2003.

[3] H. Yang, W. Hu, H. Wang, and M. Narayanan, "Investigation of reverse current for crystalline silicon solar cells—New concept for a test standard about the reverse current," in *Proc. 35th IEEE Photovolt. Specialists Conf. (PVSC)*, Jun. 2010, pp. 002806–002810.

[4] S. Silvestre and A. Chouder, "Shading effects in characteristic parameters of PV modules," in *Proc. Spanish Conf. Electron Devices*, Feb. 2007, pp. 116–118.

[5] J. W. Bishop, "Computer simulation of the effects of electrical mismatches in photovoltaic cell interconnection circuits," *Solar Cells*, vol. 25, no. 1, pp. 73–79, 1988.

[6] S. Wendlandt, A. Drobisch, T. Buseth, S. Krauter, and P. Grunow, "Hot spot risk analysis on silicon cell modules," in *Proc. 25th Eur. Photovolt. Solar Energy Conf. Exhibit.*, 2010, pp. 4002–4006.

[7] A. Simo and S. Martinuzzi, "Hot spots and heavily dislocated regions in multicrystalline silicon cells," in *Proc. Conf. Rec. 21st IEEE Photovolt. Specialists Conf. (PSC)*, May 1990, pp. 800–805.

[8] Y. Liu, B. Li, and D. Zhong, "Research on domestic PV module structure based on fault detection," in *Proc. 8th World Congr. Intell. Control Autom. (WCICA)*, Jul. 2010, pp. 171–175.

[9] Y. Liu, B. Li, and Z. Cheng, "Research on PV module structure based on fault detection," in *Proc. Chin. Control Decision Conf. (CCDC)*, May 2010, pp. 3891–3895.

[10] D. Giaffreda, M. Omaña, D. Rossi, and C. Metra, "Model for thermal behavior of shaded PV cells under hot-spot condition," in *Proc. IEEE Int. Symp. Defect Fault Tolerance VLSI Nanotechnol. Syst. (DFT)*, Oct. 2011, pp. 252–258.

[11] Z. Mei-xia and Y. Xiu, "Efficiency optimization of photovoltaic arrays based on distributed max power point tracking," in *Proc. IEEE Innov. Smart Grid Technol.-Asia (ISGT Asia)*, May 2012, pp. 1–6.

[12] R. Ramaprabha and B. L. Mathur, "Development of an improved model of SPV cell for partially shaded solar photovoltaic arrays," *Eur. J. Sci. Res.*, vol. 47, no. 1, pp. 122–134, 2010.

[13] J. A. Gow and C. D. Manning, "Development of a photovoltaic array model for use in power electronics simulation studies," *IEE Proc.-Electr. Power Appl.*, vol. 146, no. 2, pp. 193–200, Mar. 1999.

[14] P. Junsangsri and F. Lombardi, "Time/temperature degradation of solar cells under the single diode model," in *Proc. IEEE 25th Int. Symp. DFT VLSI Syst.*, Oct. 2010, pp. 240–248.

[15] P. Junsangsri and F. Lombardi, "Double diode modeling of time/temperature induced degradation of solar cells," in *Proc. 53rd IEEE Int. Midwest Symp. Circuits Syst. (MWSCAS)*, Aug. 2010, pp. 1005–1008.

[16] M. Danner and K. Bucher, "Reverse characteristics of commercial silicon solar cells-impact on hot spot temperatures and module integrity," in *Proc. 26th IEEE Photovolt. Specialists Conf.*, Oct. 1997, pp. 1137–1140.

[17] T. Shimizu, M. Kamezawa, and H. Watanabe, "Generation control circuit for photovoltaic modules," *IEEE Trans. Power Electron.*, vol. 16, no. 3, pp. 293–300, May 2001.

[18] R. Candela, V. D. Dio, E. R. Sanseverino, and P. Romano, "Reconfiguration techniques of partial shaded PV systems for the maximization of electrical energy production," in *Proc. IEEE Int. Conf. Clean Electr. Power (ICCEP)*, May 2007, pp. 716–719.

[19] A. Bidram, A. Davoudi, and R. S. Balog, "Control and circuit techniques to mitigate partial shading effects in photovoltaic arrays," *IEEE J. Photovolt.*, vol. 2, no. 4, pp. 532–546, Oct. 2012.

[20] J. Wohlgemuth and W. Herrmann, "Hot spot tests for crystalline silicon modules," in *Proc. 21st IEEE Photovolt. Specialists Conf. (PSC)*, Jan. 2005, pp. 1062–1063.

[21] S. Armstrong and W. G. Hurley, "A thermal model for photovoltaic panels under varying atmospheric conditions," *Appl. Thermal Eng.*, vol. 30, nos. 11–12, pp. 1488–1495, 2010.

[22] W. Knaupp, "Evaluation of PV module designs at irregular operation conditions," in *Proc. 26th IEEE Photovolt. Specialists Conf.*, Oct. 1997, pp. 1213–1216.

[23] J. Hudson, L. Vasilyev, J. Smidt, and G. Horner, "Economic impacts and approaches to address hot-spot defects in photovoltaic devices," in *Proc. 35th IEEE Photovolt. Specialists Conf.*, Jun. 2010, pp. 1706–1709.

[24] D. Giaffreda *et al.*, "Local shunting in multicrystalline silicon solar cell: Distributed electrical simulations and experiments," *IEEE J. Photovolt.*, vol. 4, no. 1, pp. 40–47, Jan. 2014.

[25] C. Xiao, L. Zhao, T. Asada, W. G. Odendaal, and J. D. van Wyk, "An overview of integratable current sensor technologies," in *Proc. Conf. Rec. Ind. Appl. Conf.*, vol. 2. Oct. 2003, pp. 1251–1258.

[26] K. H. Hussein, I. Muta, T. Hoshino, and M. Osakada, "Maximum photovoltaic power tracking: An algorithm for rapidly changing atmospheric conditions," *IEE Proc. Generat., Transmiss. Distrib.*, vol. 142, no. 1, pp. 59–64, 1995.

[27] T. Y. Lo and C. C. Hung, "1.5-V linear CMOS OTA with-60dB IM3 for high frequency applications," in *Proc. IEEE Solid-State Circuits Conf.*, Nov. 2006, pp. 167–170.

Daniele Rossi received the Laurea degree in electronic engineering and the Ph.D. degree in electronic engineering and computer science from the University of Bologna, Bologna, Italy, in 2001 and 2005, respectively.

He is currently a Postdoctoral Fellow with the University of Bologna. His current research interests include fault modeling and fault tolerance, coding techniques for fault-tolerance and low power, signal integrity for communication infrastructures, and robust design for soft error resiliency.

Martin Omaña received the Laurea degree in electronic engineering from the University of Buenos Aires, Buenos Aires, Argentina, in 2000 and the Ph.D. degree in electronic engineering and computer science from the University of Bologna, Bologna, Italy, in 2005.

He joined the University of Bologna in 2002, where he is currently a Postdoctoral Fellow. His current research interests include fault modeling, on-line test, robust design, fault-tolerance, and photovoltaic systems.

Dr. Omaña was a recipient of a MADESS Grant in 2002.

Daniele Giaffreda received the M.S. degree in electronic engineering from the University of Bologna, Bologna, Italy, in 2009, where he is currently working toward the Ph.D. degree with the Advanced Research Center on Electronic Systems for Information and Communication Technologies.

His current research interests include fault modeling and electrical simulations with particular emphasis on the silicon photovoltaic solar cell.

Cecilia Metra (F'14) is a Professor of Electronics with the University of Bologna, Bologna, Italy. Her current research interests include fault modeling, on-line test, robust design, fault tolerance, energy harvesting, and photovoltaic systems.

Prof. Metra is the Vice President for Technical and Conference Activities of the IEEE Computer Society (CS) for 2014, and a member of the Board of Governors of the IEEE CS from 2013 to 2015. Since 2013, she has been the Editor-in-Chief of the IEEE CS online publication computing. She is a Golden Core Member of the IEEE CS.